



## Research paper

# Early blood-brain barrier dysfunction predicts neurological outcome following aneurysmal subarachnoid hemorrhage



Svetlana Lublinsky<sup>a</sup>, Sebastian Major<sup>b,c,d</sup>, Vasilis Kola<sup>b</sup>, Viktor Horst<sup>b</sup>, Edgar Santos<sup>e</sup>, Johannes Platz<sup>f</sup>, Oliver Sakowitz<sup>e,g</sup>, Michael Scheel<sup>h</sup>, Christian Dohmen<sup>i</sup>, Rudolf Graf<sup>j</sup>, Hartmut Vatter<sup>k</sup>, Stefan Wolf<sup>l</sup>, Peter Vajkoczy<sup>b,l</sup>, Ilan Shelef<sup>a,m</sup>, Johannes Woitzik<sup>b,l</sup>, Peter Martus<sup>n</sup>, Jens P. Dreier<sup>b,c,d,o,p,1</sup>, Alon Friedman<sup>a,q,\*</sup>

<sup>a</sup> Departments of Brain & Cognitive Sciences, Physiology & Cell Biology, Faculty of Health Science, Zlotowski Center for Neuroscience, Ben-Gurion University of the Negev, Beer-Sheva, Israel

<sup>b</sup> Center for Stroke Research Berlin, Charité – Universitätsmedizin Berlin, Berlin, Germany

<sup>c</sup> Department of Experimental Neurology, Charité – Universitätsmedizin Berlin, Berlin, Germany

<sup>d</sup> Department of Neurology, Charité – Universitätsmedizin Berlin, Berlin, Germany

<sup>e</sup> Department of Neurosurgery, University Hospital Heidelberg, Ruprecht-Karls-University Heidelberg, Germany

<sup>f</sup> Department of Neurosurgery, Goethe-University, Frankfurt, Germany

<sup>g</sup> Neurosurgery Center Ludwigsburg-Heilbronn, RKH Klinikum Ludwigsburg, Ludwigsburg, Germany

<sup>h</sup> Department of Neuroradiology, Charité – Universitätsmedizin Berlin, Berlin, Germany

<sup>i</sup> LVR-Klinik Bonn, Kaiser-Karl-Ring 20, 53111 Bonn, Germany

<sup>j</sup> Multimodal Imaging of Brain Metabolism, Max-Planck-Institute for Metabolism Research, Cologne, Germany

<sup>k</sup> Department of Neurosurgery, University Hospital and University of Bonn, Bonn, Germany

<sup>l</sup> Department of Neurosurgery, Charité – Universitätsmedizin Berlin, Berlin, Germany

<sup>m</sup> Department of Diagnostic Imaging, Soroka University Medical Center, Zlotowski Center for Neuroscience, Ben-Gurion University of the Negev, Beer-Sheva, Israel

<sup>n</sup> Institute for Clinical Epidemiology and Applied Biometry, University of Tübingen, Germany

<sup>o</sup> Bernstein Center for Computational Neuroscience Berlin, Berlin, Germany

<sup>p</sup> Einstein Center for Neurosciences Berlin, Berlin, Germany

<sup>q</sup> Department of Medical Neuroscience and Brain Repair Center, Dalhousie University, Halifax, Nova Scotia, Canada

## ARTICLE INFO

## Article history:

Received 5 November 2018

Received in revised form 28 April 2019

Accepted 28 April 2019

## Keywords:

Aneurysmal subarachnoid hemorrhage  
Blood-brain barrier  
Extended Glasgow outcome scale (eGOS)  
Magnetic resonance imaging (MRI)  
Lesion  
Long term output

## ABSTRACT

**Background:** Disease progression and delayed neurological complications are common after aneurysmal subarachnoid hemorrhage (aSAH). We explored the potential of quantitative blood-brain barrier (BBB) imaging to predict disease progression and neurological outcome.

**Methods:** Data were collected as part of the Co-Operative Studies of Brain Injury Depolarizations (COSBID). We analyzed retrospectively, blinded and semi-automatically magnetic resonance images from 124 aSAH patients scanned at 4 time points (24–48 h, 6–8 days, 12–15 days and 6–12 months) after the initial hemorrhage. Volume of brain with apparent pathology and/or BBB dysfunction (BBBD), subarachnoid space and lateral ventricles were measured. Neurological status on admission was assessed using the World Federation of Neurological Societies and Rosen-Macdonald scores. Outcome at ≥6 months was assessed using the extended Glasgow outcome scale and disease course (progressive or non-progressive based on imaging-detected loss of normal brain tissue in consecutive scans). Logistic regression was used to define biomarkers that best predict outcomes. Receiver operating characteristic analysis was performed to assess accuracy of outcome prediction models.

**Findings:** In the present cohort, 63% of patients had progressive and 37% non-progressive disease course. Progressive course was associated with worse outcome at ≥6 months (sensitivity of 98% and specificity of 97%). Brain volume with BBBD was significantly larger in patients with progressive course already 24–48 h after admission (2.23 (1.23–3.17) folds, median with 95%CI), and persisted at all time points. The highest probability of a BBB-disrupted voxel to become pathological was found at a distance of ≤1 cm from the brain with apparent pathology (0.284 (0.122–0.594),  $p < 0.001$ , median with 95%CI). A multivariate logistic regression model revealed power for BBBD in combination with RMS at 24–48 h in predicting outcome (ROC area under the curve = 0.829,  $p < 0.001$ ). **Interpretation:** We suggest that early identification of BBBD may serve as a key predictive biomarker for neurological outcome in aSAH.

**Fund:** Dr. Dreier was supported by grants from the Deutsche Forschungsgemeinschaft (DFG) (DFG DR 323/5-1 and DFG DR 323/10-1), the Bundesministerium für Bildung und Forschung (BMBF) Center for Stroke Research Berlin 01 EO 0801 and FP7 no 602150 CENTER-TBI.

\* Corresponding author at: Department of Physiology & Cell Biology, Faculty of Health Sciences, Ben-Gurion University of the Negev, Beer-Sheva 84105, Israel.

E-mail address: [alonf@bgu.ac.il](mailto:alonf@bgu.ac.il) (A. Friedman).

<sup>1</sup> These authors contributed equally

Dr. Friedman was supported by grants from Israel Science Foundation and Canada Institute for Health Research (CIHR). Dr. Friedman was supported by grants from European Union's Seventh Framework Program (FP7/2007–2013; grant #602102).

© 2019 The Author(s). Published by Elsevier B.V. This is an open access article under the CC BY-NC-ND license (<http://creativecommons.org/licenses/by-nc-nd/4.0/>).

## Research in context

### Evidence before this study

We searched PubMed for articles published in any language about the effect of blood-brain barrier (BBB) damage seen on magnetic resonance imaging (MRI) of aneurysmal subarachnoid hemorrhage (aSAH) patients on risk for long-term neurological deficit. We used the search terms “blood-brain barrier”, “BBB”, “Magnetic Resonance Imaging”, “MRI”, “subarachnoid hemorrhage”, “SAH”, “lesion”, “edema”, “ischemia”, “infarction”, “outcome”, “eGOS”, “GOS”, “Glasgow Coma Scale”, and “Glasgow Outcome Scale”. Our last search was done on September 18, 2018. We found only one pilot work that was published on 6 March 2018. It reported that in a small cohort of patients ( $n = 16$ ), blood-brain barrier (BBB) permeability imaging could predict the occurrence of delayed cerebral ischemia within 14 days of aSAH. No quantitative assessment of delayed cerebral ischemia was provided. Overall, we found no reports that provide quantitative characterization of the dynamics of BBB dysfunction together with quantified dynamics of brain pathology and clinically-based assessment of disease progression in patients with acute aSAH.

### Added value of this study

This study used a large multicenter cohort of 1643 brain MR images from 124 aSAH patients imaged sequentially for over 6 months, to test the potential of quantitative BBB imaging as a prognostic and diagnostic biomarker for disease progression and neurological outcome. The strength of our study is the use of imaging-based quantitative approaches for a better understanding of the pathogenesis of neurological complications following brain injury within the clinical setting. For the first time, we identify apparently normal brain voxels that show a leaky barrier and are at risk to become pathological. We further show that a significant BBB pathology can be detected as early as 24–48 h after the acute injury. BBB pathology was most likely found in the apparently normal brain tissue surrounding the pathological brain, indicating that this adjacent tissue is at the highest risk for delayed injury. Importantly, we found BBB pathology to persist for months after the insult and was significantly more extensive in patients with a progressive disease, anatomically (MRI-based) and functionally (clinical outcome). This is the first study to propose a clinically applicable, quantitative approach for MRI imaging that detects microvascular pathology for early prediction of patients' outcome with high sensitivity and specificity. Since similar pathogenic mechanisms are involved in other brain injuries, we suggest imaging of BBB pathology as a potential novel diagnostic and predictive biomarker in brain injuries.

### Implications of all the available evidence

Due to high mortality and morbidity, accurate prognosis of aSAH patients is crucial for the identification of patients at high risk for delayed neurological complications. Specifically, there is an

unmet need for biomarkers that are related to disease pathophysiological mechanisms and may be monitored during treatment. We describe, for the first time, that a leaky BBB, detected as early as 24–48 h after the acute event, is associated with disease progression. We propose BBB pathology as a potential early biomarker for the identification of patients at high risk for disease complications and progression. Our study lays the foundation for a novel prognostic utility, employing MRI-based quantitative analysis, to significantly improve the capacity of the widely used grading systems to identify patients at high risk for disease progression. Our study suggests investigating microvascular pathology a leaky BBB as potential novel therapeutic targets in brain injury.

## 1. Introduction

Aneurysmal subarachnoid hemorrhage (aSAH) is a devastating brain insult associated with high morbidity and mortality. The incidence of aSAH is at 9·1 cases per 100,000 patient years [1] with a death rate of 40–50% [2]. Of those who survive, >40% will have long-term neurological sequelae, and less than a fifth will have no residual symptoms [3]. Due to the high mortality and morbidity rates, understanding the pathophysiology of delayed neurological complications following aSAH and identification of measurable associated biomarkers are crucial for the detection of patients at high risk for such complications, testing novel treatments and improving outcome [4].

Cerebral edema is often seen in CT or MR images of patients with aSAH and other types of brain injuries. Brain edema is a predominant cause of poor clinical outcome. The two main types are cytotoxic and vasogenic edema [5]; the latter is primarily attributed to breakdown and dysfunction of the blood-brain barrier (BBB) [6]. BBB dysfunction (BBBD) has been described within hours after aSAH and has been linked with pathologic changes such as brain edema, thrombosis, inflammation and abnormal cerebral metabolism [7–10]. BBBD has also been associated with delayed ischemia in aSAH patients [11], and the development of epilepsy and neurodegeneration after traumatic brain injury [12,13]. Accumulating pre-clinical data show that prolonged breakdown of the BBB underlies astroglial activation, neuroinflammation, neural network reorganization, dysfunction and degeneration [12,14,15]. These data suggest BBBD as a potential early prognostic biomarker after brain injury. Previously, BBB function was assessed either using statistical comparison between images acquired before and after injection of the normally non-permeable gadolinium-based contrast agent [16,17], or by dynamic studies following the kinetics of gadolinium brain concentrations [18–21]. However, such assessment has not yet been introduced in the routine clinical setting, and the hypothesis on the role of BBBD in complications after injury has not been challenged.

Along with BBBD, MR imaging in brain injured patients is often characterized by the appearance of abnormal brain tissue (ABT), which reflects cytotoxic or vasogenic edemas, gliosis or hemorrhage. Our main goal in the present study was to quantitatively characterize the dynamics of BBB dysfunction following aSAH, and assess its prognostic value using imaging- and clinically-based measures for disease progression. To this end, we developed an MRI-based quantitative approach for the identification of brain voxels with apparent ABT and BBBD. We

implemented our approach in 1643 brain MR images from 124 aSAH patients. To our knowledge, this is the first study to quantitatively assess *ABT* dynamics and the potential of *BBB* dysfunction as a predictive biomarker.

## 2. Materials and methods

### 2.1. Study design

The study was designed and performed as a longitudinal sub-study within the framework of the Co-Operative Studies of Brain Injury Depolarizations (COSBID). Patients with aSAH were selected from a prospectively collected database using pre-specified criteria and endpoints, as described below. The protocol was approved by the ethics committees of the Charité University Medicine Berlin, the Goethe-University Frankfurt, the University Hospital Heidelberg and the University of Cologne. Research was conducted in accordance with the Declaration of Helsinki. Patients or their legal representative gave written consent for study inclusion. Results are reported in accordance with the STrengthening the Reporting of OBservational studies in Epidemiology (STROBE) guidelines.

Prospective inclusion criteria for aSAH patients in COSBID have been described elsewhere [22]: (i) age ( $\geq 18$  years); (ii) World Federation of Neurosurgical Societies (WFNS) grade I–V; (iii) ruptured saccular aneurysm proven by computed tomography (CT)-angiography or digital subtraction angiography; (iv) symptom onset within the preceding 72 h; and (v) either surgical treatment of the aneurysm via craniotomy or, in coiled patients, burr hole trepanation for placement of a ventricular drain or oxygen sensor, which allows the simultaneous placement of a subdural electrode strip [23]. Exclusion criteria were subarachnoid hemorrhage due to other causes (e.g., trauma, fusiform or mycotic aneurysm), admission in a clinical state with unfavorable prognosis (e.g., wide, nonreactive pupils for  $>1$  h), bleeding diathesis or pregnancy, unavailability of the monitoring equipment and refusal of the patient or legal representative to participate in the study.

For the present study, patients were retrospectively screened for the availability of at least two serial MRI scans including a T2-weighted fluid-attenuated inversion recovery (FLAIR) sequence, a T1-weighted (T1w) 3D high-resolution sequence (i.e. magnetization prepared rapid gradient echo), a diffusion weighted imaging (DWI) sequence, and T1w sequences before and 5 min after the injection of gadolinium-DTPA (Gd-DTPA 0.5 M, 0.1 mmol/kg).

One hundred twenty-four patients enrolled between January 2007 and March 2016 met criteria, including 50 at Campus Virchow Klinikum, 44 at Campus Benjamin Franklin (Charité University Medicine Berlin), 18 at the Goethe-University Frankfurt, 6 at the University of Cologne and 6 at the University Hospital Heidelberg.

Retrospective analysis of MR images was performed blindly on 377 examinations from the 124 aSAH patients, as well as on images from 21 healthy controls. Each patient had between two and four MRI examination visits and was imaged sequentially for  $>6$  months. Details of the sequences are provided in appendix Table 1.

Since the longitudinally collected imaging datasets of aSAH patients accommodated an unequal number of follow-up scans per subject and unequal time intervals between scans, we categorized scans according to the time windows after aneurysm event as follows: acute: 24–48 h ( $t1$ ), sub-acute: 3–9 days ( $t2$ ), delayed: 10–19 days ( $t3$ ), and late, around one year (267.6(196.6–358.2); range of 59–1472 days) ( $t4$ ) after the initial hemorrhage. Availability of clinical data and the number of imaging sets available for analysis at each time point are presented in Tables 1 and 2.

### 2.2. Clinical data

Obtained data included location of aneurysm; type of intervention; vasospasm identification; history of arterial hypertension, anemia on

admission anemia on admission defined as total hemoglobin  $<14$  g/dl in males and  $<12$  g/dl in females, abnormal liver enzymes on admission defined as alanine aminotransferase (ALT)  $>45/34$  U/L (male/female), aspartate aminotransferase (AST)  $>50/35$  U/L or gammaglutamyl transferase (GGT)  $>55/38$  U/L; history of previous aSAH; World Federation of Neurosurgical Societies (WFNS) scale [24] and Rosen-Macdonald Score (RMS) [25] at admission and extended Glasgow Outcome Scale (eGOS) measured at  $t4$ , as mentioned above. Significant proximal vasospasm (V+) was defined using Doppler sonography, if mean velocity was  $>200$  cm/s in at least one middle cerebral artery (MCA). Vasospasm (V-) was excluded if the MCA mean velocities remained  $<120$  cm/s and was defined as possible/not excluded (V-/+ ) when mean velocity was between 120 and 200 cm/s [26]. WFNS and RMS data on admission were categorized into favorable (WFNS  $<4$ , RMS  $\leq 4$ ) or poor (WFNS  $\geq 4$ , RMS  $> 4$ ). Poor outcome was defined as eGOS  $\leq 5$  (severe disability or death) and favorable outcome as eGOS  $>5$  (no or moderate disability).

### 2.3. Image analysis

MR images (including T1w, FLAIR and DWI sequences) were automatically segmented into apparently normal brain tissue (NBT) in the combined gray matter (GM) and white matter (WM), lateral ventricles (LV) and subarachnoid space (SAS), or *ABT* comprising apparently abnormal signal, reflecting cytotoxic or vasogenic edema, gliosis or hemorrhage. Image processing methods, including multimodal normal tissue and *ABT* segmentation, *BBB* permeability evaluation, and *ABT* vicinity analysis, are provided in the appendix. Prediction of *ABT* volume at long-term outcome, assessment of *BBBD* persistency over time, and evaluation of *BBBD* predictive properties in *ABT* progression and long-term clinical outcomes are provided in the appendix.

### 2.4. Patient classification based on imaging-detected loss of normal brain tissue in consecutive scans

Because intracranial volume is fixed, the increase in *ABT* and/or enlargement of *LV* and *SAS* were associated with decrease in *NBT* volume. Such decrease in consecutive scans was attributed to disease “progressive course” (PC), while no change, or increase in *NBT* volume was considered as a “non-progressive course” (NPC) (see appendix).

### 2.5. Statistical analysis

Quantitative and ordinal data are presented as median with inter-quartile range and categorical variables are presented as values and percentages. The  $\chi^2$  and Fisher's exact (employing Monte Carlo method) tests (for contingency table  $>2 \times 2$ ) were used to analyze categorical variables. The Wilcoxon rank-sum test was used to analyze continuous independent variables between two groups. A non-parametric Kruskal-Wallis test was performed for continuous independent variables to test the overall multiple group ( $>2$ ) differences. The Wilcoxon sign-rank test and Friedman test were used for comparison of dependent variables. When the overall comparisons between different time points were significant, post-hoc tests for multiple comparison correction were performed using Bonferroni procedure. Univariate-logistic regression analysis was used to identify possible risk factors for outcomes of aSAH and odds ratios including 95% confidence intervals were presented. The possible risk factors were included in the multivariate logistic regression analysis for outcomes prediction. Variable selection (forward, inclusion  $p = .05$ , exclusion  $p = .10$ ) was applied. Receiver operating characteristic (ROC) analysis was performed to assess the diagnostic accuracy of outcome prediction models [27]. The level of significance was 0.05 (two-sided) in all analyses.

**Table 1**  
Clinical data: Demographic data, characteristics of disease and intervention<sup>a</sup>.

	eGOS ≤ 5 (n = 69, 61.6%) <sup>b</sup>	eGOS > 5 (n = 43, 38.4%) <sup>b</sup>	OR (95% CI)	p-value	PC (n = 78, 62.9%)	NPC (n = 46 37.1%)	OR (95% CI)	p-value
Sex				0.6757				0.5524
Female	46	31	..		51	33	..	
Male	23	12	..		27	13	..	
Neurological score at admission								
WFNS ≥ 4	46	14	4.14 (1.84–9.32)	0.0005	49	17	3.31 (1.46–6.52)	0.0018
WFNS < 4	23	29			29	31		
RMS > 4	63	23	9.13 (3.26–25.57)	0.0000	68	27	4.79 (1.97–11.61)	0.0004
RMS ≤ 4	6	20			10	19		
Aneurysm location <sup>c</sup>				0.7695				0.8350
ACA	3	2	..		3	2	..	
MCA	26	15	..		29	18	..	
ICA	3	4	..		4	4	..	
ACoP	11	6	..		12	6	..	
ACoA	21	14	..		25	14	..	
PeriA	0	1	..		0	1	..	
BCA	3	0	..		3	0	..	
PICA	2	1	..		2	1	..	
Type of intervention				0.7631				0.5683
Clipping	60	39	0.68 (0.20–2.37)		68	42	0.65 (0.19–2.20)	
Coiling	9	4			10	4		
Presence of vasospasm				0.2946				0.1347
V-	17	12	..		19	16	..	
V-/+	21	18	..		23	17	..	
V+	31	13	..		36	13	..	
Arterial hypertension <sup>d</sup>				0.0013				0.0153
True	40	13	3.69 (1.63–8.39)		42	16	2.46 (1.15–5.27)	
Not true	25	30			32	30		
Anemia <sup>d</sup>				0.0266				0.0309
True	17	3	3.98 (1.06–15.00)		18	3	3.77 (1.01–14.01)	
Not true	37	26			43	27		
Abnormal liver enzymes <sup>d</sup>				0.4688				0.3716
True	19	8	..		23	8	..	
Not true	38	19	..		41	19	..	
Uric acid <sup>d</sup>				0.5021				0.2708
Below normal	24	11	..		29	9	..	
Normal	19	10	..		20	10	..	
Total cholesterol <sup>d</sup>				0.9686				0.9811
Evaluated	1	2	..		1	2	..	
Normal	38	17	..		43	15	..	
Previous aSAH				1.0000				1.0000
True	0	1	..		0	1	..	
Not true	69	42	..		78	45	..	

OR = odds ratio. PC = progressive course of aSAH. NPC = non-progressive course of aSAH.

<sup>a</sup> Only significant OR values were presented in the table.<sup>b</sup> Neurological outcome (eGOS) was available for 112 (90%) patients.<sup>c</sup> Aneurysms were assessed using four-vessel digital subtraction angiography (DSA).<sup>d</sup> Clinical data were not available for all of the patients.

### 3. Results

#### 3.1. Clinical findings, demographics and outcome of aSAH patients

Overall, clinical, demographic and imaging data were analyzed from 124 aSAH patients, including 84 women (67.7%) and 40 men, admitted to 5 medical centers between 2007 and 2016 (appendix, Table 1). Mean age of patients was  $55.2 \pm 11.3$  years (range, 22–79 years). We also scanned 21 healthy control subjects,  $28.1 \pm 14.7$  years (range, 19–46 years). Females were significantly older at the time of admission compared to males (56 (49–64) vs. 50 (44–60.5) years,  $p < 0.001$ , Wilcoxon test). The most frequent locations of aneurysm were middle cerebral artery (MCA) (47/124, 37.9%), anterior communicating artery (ACoA) ( $n = 39$ , 31.5%) and posterior communicating artery ( $n = 18$ , 14.5%). Among females, most were along the MCA (45.2% compared to 22.5% in males,  $p = 0.025$ ,  $\chi^2$  test), while ACoA aneurysms were more common in males (50.0% compared to 22.6% in females,  $p = 0.004$ ,  $\chi^2$  test). Other locations showed no statistically significant difference between both genders ( $p > 0.4$ ,  $\chi^2$  test). Near-significant association was found between age and aneurysm location ( $p = 0.063$ , Kruskal-Wallis, patients with MCA aneurysm were younger 51

(46–59) years, than patients with anterior communicating artery (ACA) aneurysm 69 (59–72) years,  $n = 5$ ). Patients were either treated with surgical clipping (110, 88.7%) or coiling (14, 11.3%). No statistically significant relationships were found between the intervention type and age ( $p > 0.4$ ), gender ( $p = 0.377$ ,  $\chi^2$  test), aneurysm location ( $p > 0.7$ , Fisher's test) or presence of vasospasm ( $p > 0.4$ , Fisher's test).

No statistically significant relationships were found between WFNS score on admission and gender ( $p = 0.294$ ,  $\chi^2$  test), age ( $p = 0.305$ , Wilcoxon test), aneurysm location ( $p = 0.680$ , Fisher test), type of treatment ( $p = 0.333$ ,  $\chi^2$  test) or presence of vasospasm ( $p = 0.264$ , Fisher test). Similarly, no statistically significant relationships were found between RMS score on admission and gender ( $p = 0.771$ ,  $\chi^2$  test), aneurysm location ( $p = 0.299$ , Fisher test), or presence of vasospasm ( $p = 0.472$ , Fisher test). However, RMS was related to patient age ( $p < 0.001$ , Wilcoxon test).

Patients with a poor outcome (eGOS) were older than those with a favorable outcome (57 (48–65) years vs 52 (44–59) years;  $p = 0.009$ ). No statistically significant relationships were found between eGOS category and aneurysm location ( $p = 0.762$ , Fisher's test), gender ( $p = 0.604$ ,  $\chi^2$  test), intervention ( $p = 0.660$ ,  $\chi^2$  test) or presence of vasospasm ( $p = 0.743$ , Fisher's test) (Table 1).

**Table 2**  
Quantitative imaging data as related to clinical outcome†.

	eGOS ≤ 5	eGOS > 5	n of eGOS ≤ 5, n of eGOS > 5	OR (95% CI)	p-value	AUC (95% CI)	PC	NPC	n of PC, n of NC	OR (95% CI)	p-value	AUC (95% CI)
<i>Age, years</i>	57.00 (48.00–65.00)	52.00* (44.00–59.00)	69, 43	1.06 (1.02–1.10)	0.0261	0.62 (0.51–0.73)	57.00 (48.00–65.00)	52.00* (44.00–60.00)	78, 46	1.04 (1.00–1.07)	0.0351	0.62 (0.51–0.73)
<i>WFNS</i>	4 (2–5)	2* (1–4.5)	69, 43	1.60 (1.22–2.11)	0.0007	0.66 (0.55–0.77)	4 (2–5)	2 (1–4.5)*	78, 46	1.56 (1.21–2.01)	0.0005	0.65 (0.55–0.75)
<i>RMS</i>	7 (5–8)	5* [3–7]	69, 43	1.73 (1.33–2.24)	0.0002	0.75 (0.65–0.85)	7 (5–8)	5* [3–7]	78, 46	1.52 (1.22–1.90)	0.0002	0.71 (0.62–0.81)
<i>ABT volume, ml</i>												
<i>ABT<sub>1</sub></i>	85.24 (58.95–131.88)	55.82 (34.79–98.11)	69, 43	1.01 (1.00–1.02)	0.0401	0.67 (0.58–0.79)	84.31 (54.69–131.57)	56.25 (35.19–102.02)	78, 46	1.01 (1.00–1.02)	0.0410	0.66 (0.57–0.79)
<i>ABT<sub>2</sub></i>	111.46† (80.47–219.23)	68.05* (33.05–105.38)	42, 24	1.02 (1.01–1.04)	0.0040	0.74 (0.62–0.88)	109.88† (80.47–219.23)	67.46* (33.05–115.15)	47, 25	1.02 (1.01–1.03)	0.0045	0.74 (0.62–0.87)
<i>ABT<sub>3</sub></i>	134.98† (91.94–199.37)	59.75* (28.68–93.24)	62, 37	1.02 (1.01–1.04)	0.0002	<b>0.83</b> <b>(0.74–0.92)</b>	134.55† (91.42–205.27)	61.39* (30.71–102.64)	71, 40	1.02 (1.01–1.03)	0.0003	<b>0.80</b> <b>(0.71–0.89)</b>
<i>ABT<sub>4</sub></i>	138.71† (102.79–204.39)	29.55*† (15.78–73.55)	36, 33	1.03 (1.02–1.05)	0.0002	<b>0.88</b> <b>(0.81–0.97)</b>	138.66† (99.23–204.39)	29.55*† (16.92–71.70)	37, 33	1.03 (1.02–1.05)	0.0002	<b>0.88</b> <b>(0.80–0.96)</b>
<i>NBT volume, ml</i>												
<i>NBT<sub>1</sub></i>	1496.3‡ (1359.1–1568.5)	1461.8‡ (1370.5–1530.8)	69, 43	..	0.7218	..	1503.0‡ (1401.2–1575.0)	1455.6‡ (1364.4–1522.0)	78, 46	..	0.	.. 4101
<i>NBT<sub>2</sub></i>	1425.2‡ (1349.7–1534.9)	1452.0‡ (1384.1–1515.1)	42, 24	..	0.4159	..	1425.7‡ (1350.1–1534.9)	1440.8‡ (1377.1–1515.1)	47, 25	..	0.5738	..
<i>NBT<sub>3</sub></i>	1383.3‡ (1276.6–1480.7)	1451.4‡ (1373.2–1531.6)	62, 37	..	0.0869	..	1390.0 ‡ (1287.5–1495.1)	1442.5‡ (1366.6–1521.4)	71, 40	..	0.0908	..
<i>NBT<sub>4</sub></i>	1347.4‡ (1198.6–1411.8)	1475.5‡ (1410.8–1542.3)	36, 33	0.99 (0.98–1.00)	0.0025	<b>0.81</b> <b>(0.70–0.91)</b>	1351.8‡ (1198.6–1437.0)	1469.3*‡ (1389.9–1537.0)	37, 33	0.99 (0.99–1.00)	0.0055	0.77 (0.66–0.89)
<i>LV volume, ml</i>												
<i>LV<sub>1</sub></i>	36.59‡ (22.59–57.57)	35.13‡ (23.18–48.08)	69, 43	..	0.7216	..	33.81‡ (20.36–51.44)	35.18‡ (23.81–49.51)	78, 46	..	0.9792	..
<i>LV<sub>2</sub></i>	34.30‡ (18.44–50.59)	27.86 (21.31–37.19)	42, 24	..	0.8668	..	30.47‡ (17.92–49.00)	27.52‡ (21.31–37.19)	47, 25	..	0.9723	..
<i>LV<sub>3</sub></i>	40.04‡ (22.00–60.38)	35.87‡ (22.00–54.46)	62, 37	..	0.2754	..	38.29‡ (23.10–60.27)	36.32‡ (27.60–54.46)	71, 40	..	0.8910	..
<i>LV<sub>4</sub></i>	68.29‡ (47.98–108.98)	45.62*‡ (32.07–69.85)	36, 33	1.02 (1.00–1.03)	0.0153	0.67 (0.54–0.80)	71.51‡ (50.90–109.39)	44.69*‡ (30.77–56.16)	37, 33	1.03 (1.01–1.05)	0.0012	0.74 (0.62–0.86)
<i>SAS volume, ml</i>												
<i>SAS<sub>1</sub></i>	267.08‡ (154.80–379.21)	228.55‡ (150.32–344.57)	69, 43	..	0.2901	..	257.66‡ (148.10–354.18)	246.45‡ (160.75–377.70)	78, 46	..	0.8161	..
<i>SAS<sub>2</sub></i>	159.26† (107.35–296.91)	195.45 (147.68–298.13)	42, 24	..	0.3408	..	157.28† (104.13–296.91)	196.00 (147.69–319.27)	47, 25	..	0.2162	..
<i>SAS<sub>3</sub></i>	231.66‡ (154.20–337.51)	233.05‡ (145.36–349.60)	62, 37	..	0.6926	..	221.41‡ (148.19–333.90)	257.89‡ (187.68–401.95)	71, 40	..	0.5036	..
<i>SAS<sub>4</sub></i>	447.19‡ (272.10–564.83)	361.93*‡ (281.57–481.77)	36, 33	..	0.1223	..	450.92‡ (272.10–564.83)	363.43*‡ (281.57–497.71)	37, 33	..	0.1584	..
<i>ABTBBD volume, ml</i>												
<i>ABTBBD<sub>1</sub></i>	19.23 (9.53–24.57)	11.72* (9.08–22.17)	49, 30	1.06 (1.01–1.11)	0.0109	0.68 (0.55–0.80)	23.02 (12.01–31.08)	12.13* (9.23–22.83)	59, 34	1.05 (1.01–1.09)	0.0177	0.66 (0.54–0.78)
<i>ABTBBD<sub>2</sub></i>	27.60† (14.83–48.23)	19.20* (8.68–25.24)	32, 18	1.05 (1.01–1.10)	0.0184	0.69 (0.52–0.86)	39.11† (19.06–60.50)	18.80* (7.82–24.73)	35, 20	1.06 (1.01–1.11)	0.0088	0.72 (0.56–0.88)
<i>ABTBBD<sub>3</sub></i>	35.88† (23.77–56.47)	14.55* (8.84–36.32)	50, 28	1.05 (1.02–1.08)	0.0004	0.79 (0.68–0.90)	44.14† (28.15–71.10)	15.54* (8.83–37.41)	58, 30	1.05 (1.02–1.08)	0.0002	0.78 (0.67–0.89)
<i>ABTBBD<sub>4</sub></i>	19.91 (13.12–43.18)	5.90*† (2.89–13.87)	23, 21	1.07 (1.02–1.13)	0.0071	<b>0.85</b> <b>(0.73–0.97)</b>	24.38 (18.23–50.99)	5.84*† (2.89–11.33)	24, 22	1.08 (1.02–1.14)	0.0077	<b>0.85</b> <b>(0.73–0.97)</b>
<i>NBTBBD volume, ml</i>												
<i>NBTBBD<sub>1</sub></i>	127.05‡ (109.78–160.60)	106.70*‡ (62.94–128.60)	49, 30	1.02 (1.01–1.04)	0.0017	0.73 (0.61–0.82)	129.47‡ (111.38–161.72)	102.08*‡ (65.53–127.64)	59, 34	1.03 (1.01–1.04)	0.0003	0.73 (0.62–0.84)

NBTBBBD <sub>2</sub>	135·41a (90·94–180·24)	90·94*† (64·84–115·12)	32, 18	1·03 (1·01–1·05)	0·0086 <b>0·80</b> <b>(0·64–0·94)</b>	140·32‡ (104·34–191·58)	90·23*† (62·70–102·74)	35, 20	1·04 (1·02–1·07)	0·0019 <b>0·84</b> <b>(0·71–0·97)</b>
NBTBBBD <sub>3</sub>	127·72‡ (102·66–167·98)	94·63*† (72·22–110·45)	50, 28	1·02 (1·01–1·04)	0·0016 0·77 (0·65–0·88)	127·72‡ (102·66–167·98)	94·63*† (70·52–109·71)	58, 30	1·03 (1·01–1·05)	0·0002 0·77 (0·66–0·88)
NBTBBBD <sub>4</sub>	105·61†‡ (79·18–146·66)	69·87*†‡ (54·99–97·62)	23, 21	1·03 (1·01–1·05)	0·0114 0·75 (0·61–0·90)	110·68†‡ (79·21–147·64)	67·52*†‡ (54·99–92·29)	24, 22	1·04 (1·01–1·07)	0·0031 0·79 (0·65–0·93)
ABTBBBD <sup>10</sup> volume, ml										
ABTBBBD <sup>10</sup>	42·19 (28·51–60·71)	29·19* (17·29–46·95)	49, 30	1·04 (1·01–1·06)	0·0092 0·66 (0·53–0·78)	45·78 (28·68–65·18)	29·63* (18·58–45·26)	59, 34	1·04 (1·01–1·06)	0·0077 0·67 (0·54–0·79)
ABTBBBD <sup>10</sup> <sub>2</sub>	51·74 (38·48–72·96)	28·42* (15·92–47·61)	32, 18	1·05 (1·01–1·08)	0·0076 0·77 (0·62–0·93)	55·58 (40·57–74·87)	28·42* (13·77–43·44)	35, 20	1·09 (1·04–1·16)	0·0001 <b>0·81</b> <b>(0·67–0·95)</b>
ABTBBBD <sup>10</sup> <sub>3</sub>	52·14 (34·98–74·48)	28·11* (17·88–38·96)	50, 28	1·04 (1·01–1·06)	0·0022 0·76 (0·65–0·88)	52·14 (34·98–74·48)	28·11* (17·82–39·98)	58, 30	1·05 (1·02–1·07)	0·0004 0·76 (0·64–0·87)
ABTBBBD <sup>10</sup> <sub>4</sub>	36·67† (24·35–54·67)	9·98*† (6·65–23·52)	23, 21	1·08 (1·03–1·14)	0·0012 <b>0·85</b> <b>(0·73–0·97)</b>	36·66† (24·74–54·31)	9·47*† (6·65–20·89)	24, 22	1·09 (1·04–1·16)	0·0009 <b>0·87</b> <b>(0·76–0·98)</b>
ABTBBBD <sup>20</sup> volume, ml										
ABTBBBD <sup>20</sup>	38·89 (29·32–47·82)	27·50 (20·35–48·14)	49, 30	1·02 (0·99–1·05)	0·0824 0·61 (0·48–0·74)	39·16 (30·12–48·89)	30·41* (21·07–42·53)	59, 34	1·03 (1·00–1·06)	0·0264 0·64 (0·52–0·76)
ABTBBBD <sup>20</sup> <sub>2</sub>	35·51 (30·21–50·70)	28·61* (16·60–34·74)	32, 18	1·06 (1·01–1·12)	0·0225 0·76 (0·53–0·87)	35·59 (27·83–50·98)	25·02* (15·84–34·51)	35, 20	1·09 (1·03–1·16)	0·0040 0·77 (0·60–0·91)
ABTBBBD <sup>20</sup> <sub>3</sub>	33·71 (26·32–44·09)	25·64* (17·03–32·99)	50, 28	1·06 (1·02–1·11)	0·0049 0·74 (0·58–0·83)	33·71 (25·42–44·35)	25·64* (16·70–30·37)	58, 30	1·07 (1·03–1·12)	0·0013 0·74 (0·59–0·83)
ABTBBBD <sup>20</sup> <sub>4</sub>	34·60 (29·37–50·75)	18·39* (7·76–30·01)	23, 21	1·08 (1·02–1·14)	0·0039 0·79 (0·65–0·92)	34·69 (29·73–50·28)	17·94*† (7·76–28·12)	24, 22	1·10 (1·03–1·17)	0·0017 <b>0·82</b> <b>(0·67–0·95)</b>

OR = odds ratio. PC = progressive course of aSAH. NPC = non-progressive course of aSAH.

Significant difference  $\leq 0·05$  between outcome groups (eGOS  $\leq 4$ , vs eGOS  $> 4$ , or PC vs NC) with Wilcoxon sum-rank test\*. Significant difference  $\leq 0·05$  between different time points with Friedman test†. Significant difference  $\leq 0·05$  between control and a measurement at a single time point with Wilcoxon sum-rank test‡. The area under the ROC curve (AUC) results were considered “excellent” for AUC values between 0·9–1, “good” for AUC values between 0·8–0·9, “fair” for AUC values between 0·7–0·8, “poor” for AUC values between 0·6–0·7 and failed for AUC values between 0·5–0·6.

† Only significant OR values were presented in the table.

A significant association was found between presence of arterial hypertension and anemia on admission and a poor outcome ( $p = 0.0013$  and  $p = 0.0266$ ,  $\chi^2$  test, correspondently, Table 1).

### 3.2. Dynamics of intracranial measures

Volume of *ABT* was measured longitudinally in 377 imaging sets from 124 patients (Fig. 1 and appendix, Table 2). *ABT* volume in the early scan ( $t1$ , 24–48 h after event) was similar in females and males; increased with patient age; largest in patients with MCA aneurysms; significantly larger in patients with poor WFNS ( $p = 0.003$ , Wilcoxon rank-sum test) and in patients with poor outcome (Tables 1–2). *ABT* volume at  $t4$  (>6 months after event) was not significantly associated with age or aneurysm location and was significantly larger in patients with poor WFNS and with poor eGOS ( $p = 0.0002$ , Table 2). Overall, *ABT* volume significantly increased with time (Fig. 1f). As expected, change in *ABT* volume was inversely correlated with the volume of *NBT* ( $p < 0.006$ ). Interestingly, volume of CSF compartments (lateral ventricles and SAS) significantly increased only at  $t4$  ( $p < 0.001$ , Fig. 1d–e). No significant differences were found between patients who were surgically clipped or coiled ( $p > 0.6$ , Wilcoxon rank-sum test).

### 3.3. BBB dysfunction

Contrast-enhanced MRIs from 104 patients (total of 282 scans) were used to detect brain voxels with *BBBD* (Supp. Figure and Fig. 1–2a). Interestingly, most voxels with *BBBD* were found within the apparently healthy brain (Fig. 1g), indicating that despite abnormal contrast enhancement, this brain tissue does not show a pathological signal in routine MR sequences (including T1w, FLAIR and DWI). *BBBD* within the apparently healthy brain voxels was most commonly found within a 1-cm ring surrounding lesion cores (Fig. 2m).

The extent and volume of brain regions with *BBBD* were not significantly associated with gender ( $p > 0.09$ , the Mann-Whitney test), aneurysm location ( $p > 0.3$ , Kruskal-Wallis test), or treatment (clipped vs coiled,  $p > 0.7$ ). *BBBD* within the *ABT* was significantly increased at  $t2$  and  $t3$  compared to  $t1$  and was significantly reduced only in delayed scans ( $t4$ ). Within the apparently normal brain tissue, *BBBD* did not change during the first two weeks after the event ( $t1$ – $t3$ ) and significantly declined only in the late scan ( $t4$ ,  $p < 0.01$ , Friedman test, Fig. 1g). To examine the time course of *BBBD* in specific brain voxels, we calculated the probability of a voxel with *BBBD* to remain permeable. Interestingly, the probability of any brain voxel to display *BBBD* during

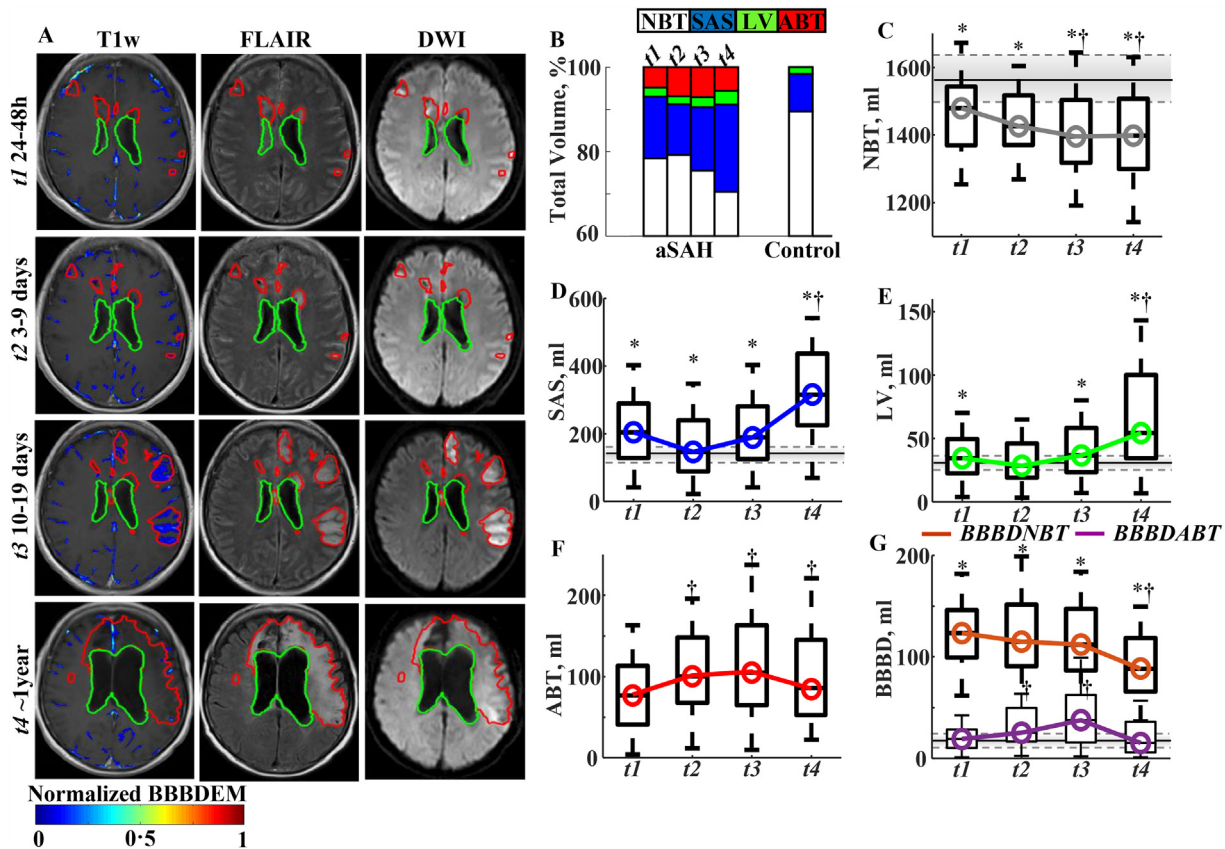


**Fig. 1.** Dynamics of brain MR findings during follow-up. a. Representing MR scans during follow-up. Detected abnormal brain tissue (*ABT*) in red contour. *BBBD* enhancement maps (*BBBDEM*) were created by reassigning each voxel with *BBBD* its enhancement level. The final *BBBDEM* was normalized to 0–1 range (minimal to maximal enhancement level). b. Bar graph showing composition of skull-peeled volume of interest at different time point during follow-up. Normal brain tissue (*NBT* - white); CSF sub-arachnoid space (*SAS* - blue); Lateral ventricles (*LV* - green); *ABT* - red. Note the gradual reduction in *NBT* during follow-up. c. Box plot showing mean *NBT* volumes in aSAH patients over time. Note a significant decrease beginning ~2 weeks after the event ( $p = 0.002$ , Friedman). d, e. Volume of *LV* (D) and *SAS* (E) showing a significant increase at  $t4$  ( $p < 0.001$ , Friedman). f. *ABT* volume significantly increased in aSAH patients at all time intervals in comparison to  $t1$  ( $p < 0.02$ ). *NBT* and *ABT* volumetric changes followed a logarithmic pattern ( $R^2_{adj} = 0.82(0.76-0.99)$  for brain volume and  $R^2_{adj} = 0.81(0.78-0.97)$  for *ABT* volume ( $p < 0.01$ ); correlation between model intercept ( $Co$ ) and *NBT* and *ABT* sizes were correspondently:  $R^2 = 0.96$  ( $p = 0.02$ ) and  $R^2 = 0.88$  ( $p = 0.01$ )). Dynamic of *ABT* and *BBBD* in a subgroup with all four time points is presented in Supplementary Fig. 3. g. Brain volume with *BBBD* within the “abnormal” brain (*ABTBBBD*) significantly increased in  $t2$  and  $t3$  compared to  $t1$  followed by a significant reduction at  $t4$  (lilac color). *BBBD* within the *NBT* (brown color) was 3–2 (0.8–10.8) fold greater compared to that in healthy controls at all the investigated time intervals  $t1$ – $t4$  ( $p < 0.001$ ). Notably, brain volume with *BBBD* within the *NBT* persisted during the first two week after the acute bleeding event and was significantly reduced only at  $t4$  ( $p < 0.01$ ). Overall, *NBT* brain volume with *BBBD* was larger compared to that measured in controls at all-time points. Control data are represented by horizontal solid (median) and dash (third and first quartiles) lines. †Significant difference ( $p \leq 0.05$ ) between time points (Friedman test followed the Bonferroni procedure). \*Significant difference ( $p \leq 0.05$ ) between control and aSAH patients at a single time point (Wilcoxon rank sum test). *ABT* = abnormal brain tissue; aSAH = aneurysmal subarachnoid hemorrhage; *BBBD* = blood brain barrier damage; *ABTBBBD* = blood brain barrier damage measured in abnormal brain tissue volume; *NBTBBBD* = blood brain barrier damage measured in normal brain tissue volume; *LV* = lateral ventricles; *NBT* = normal brain tissue; *SAS* = subarachnoid space.

the first week after the acute bleeding ( $p_{1,2}^{BBBD}=0.370(0.274-0.587)$ ) was not significantly different from that measured during the second week ( $p_{2,3}^{BBBD}=0.382(0.311-0.412)$ ) and significantly lower only at delayed time points,  $t_3$  and  $t_4$  ( $p_{3,4}^{BBBD}=0.238(0.176-0.365)$ ),  $p = 0.005$ , Friedman test).

To test the predictive value of *BBBD*, we examined the outcome of a *BBB*-disrupted voxel within healthy brain tissue. Results showed that a *NBT* voxel with *BBBD* had a significantly higher probability to become abnormal (*ABT*) compared to a voxel with intact *BBB* ( $p < 0.001$ , Wilcoxon rank-sum test, Table 3). These results highlight *BBBD* as a potential early predictive biomarker for brain tissue at risk. While

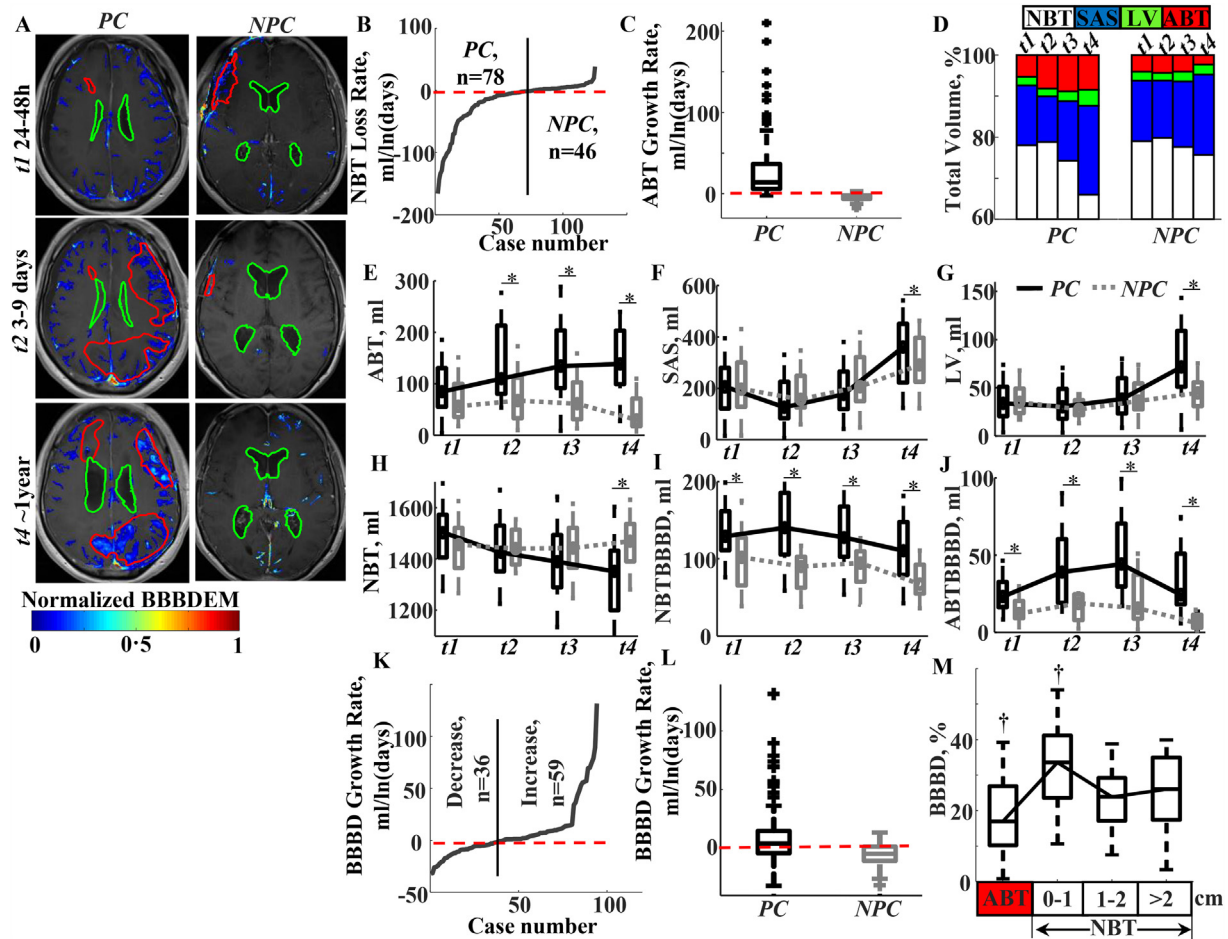


**Fig. 2.** Different BBB dynamics in patients with progressive vs non-progressive disease course. a. Representing MR images from aSAH patients with a progressive (PC) and non-progressive (NPC) disease course. *BBBD* enhancement maps (*BBBDEM*, color bar) are superimposed. Red contour demarcates detected abnormal brain tissue (*ABT*) and green contour demarcates lateral ventricles (*LV*). *BBBDEM* were created by reassigning each voxel with *BBBD* its enhancement level. The final *BBBDEM* was normalized to 0–1 range (minimal to maximal enhancement level). b. Based on measurements of changes in normal brain tissue (*NBT*) volume over time, patients were classified as having either a “progression course” (PC), in which *NBT* decreased with time ( $t_2$ – $t_4$ ) compared to the first, acute scan ( $t_1$ ) (median slope:  $-18.75 (-48.92-9.07)$  ml/ln(days)), or a “non-progression course” (NPC), characterized by *NBT* volume change slope of  $0.73 (0.06-3.58)$  ml/ln(days). c. Box plot showing a significant difference in *ABT* growth rate between PC and NPC groups:  $13.99 (5.90-36.68)$  ml/ln(days) vs  $-3.50 (-6.45-2.09)$  ml/ln(days);  $p < 0.001$ , Wilcoxon test. d. Bar graph showing the distribution in brain volume of *NBT* (white), subarachnoid space (*SAS*, blue), *LV* (green) and *ABT* (red) over time in the two patient groups. The increase in *ABT* and/or enlargement of *LV* and *SAS* were associated with decrease in *NBT* volume. The relative contributions of *ABT* growth vs *CSF* enlargement ( $LV + SAS$ ) to *NBT* atrophy was about 1:2 for PC and 1:4 for NPC patients. e. A significant increase in *ABT* volume during consecutive scans in PC patients ( $ABT_i/ABT_1 > 1$ , for  $i = 2-4$ ,  $p < 0.001$ ; see also Table 2, appendix: Table 2B). In contrast, NPC patients displayed non-significant change in *ABT* volume during the first 2 weeks (3 scans) after the acute bleeding event and a significant decrease in *ABT* volume by  $t_4$  ( $p < 0.007$ ; see also appendix Table 2B). f, g. Significant differences between PC and NPC groups in both *SAS* volume (f) and *LV* volume (g) were found only in the late ( $t_4$ ) scans ( $p < 0.001$ , Wilcoxon test; see also Table 2). Note lack of significantly differences between the groups in none of the measures (*ABT*, *LV* or *SAS* volume) during the acute stage. h. Significant difference between the groups in *NBT* volume were seen only in the late ( $t_4$ ) scans ( $p < 0.001$ ; Table 2). In the PC group, a significant decrease in *NBT* was detected from ~2 weeks after the event ( $p < 0.01$ , Friedman). i, j. Volumes of *BBBD* in both *NBT* (i, *NBTBBBD*) and *ABT* (i, *ABTBBBD*) were persistently and significantly greater in the PC group relative to NPC group in all time points ( $p < 0.001$ , Wilcoxon test, see also Table 2). In both groups, a significant decrease in *NBTBBBD* was seen only by  $t_4$  ( $p < 0.001$ , Friedman), whereas *ABTBBBD* increased significantly between  $t_2$ – $t_3$  in PC group, and decreased significantly by  $t_4$  in NPC group ( $p < 0.001$ , Friedman). Resolution of *BBBD* to 95% CI values of “healthy controls” ( $<47.5$  ml) was found only in three patients. All these three patients were in NPC group and had *ABT* size significantly smaller than patients with non-resolved *BBBD* throughout the investigation. Overall, *NBTBBBD* volume was larger in both groups compared to that measured in controls at all time points (Table 2). k. Overall, in 62% of aSAH patients brain volume with *BBBD* (*NBTBBBD* + *ABTBBBD*) increased with time (slope:  $8.57(2.02-24.64)$  ml/ln(days)) and in 38% of patients *BBBD* decreased with time (slope:  $-8.95(-16.87-5.07)$  ml/ln(days)). l. Box plot showing a significant difference in *BBBD* growth rate between PC and NPC groups:  $3.93 (-4.44-16.78)$  ml/ln(days) vs  $-4.73 (-10.74-1.32)$  ml/ln(days),  $p = 0.001$ , Wilcoxon test). Interestingly, while in 64% of the patients from the PC group brain volume with *BBBD* increased with time, in 76% of patients in the NPC group *BBBD* decreased with time ( $p = 0.022$ ,  $\chi^2$  test). m. Box plot of the distribution of *BBBD* in abnormal and apparently normal brain tissue, where it was measured in three regions of interest based on the distance to *ABT* border (in cm). *BBBD* voxels were not distributed equally through all regions ( $p < 0.001$ ). The highest content of *BBBD* voxels was found within 1 cm of *ABT* ( $33.58 (23.66-41.18)$  % of entire *BBBD* volume), whereas the lowest content of *BBBD* voxels was located in *ABT* ( $16.98 (10.25-26.92)$  % of entire *BBBD* volume). No significant difference was found in content of *BBBD* between the two remaining regions (1–2 cm and  $> 2$  cm from *ABT* border):  $23.90 (17.17-29.27)$  % and  $25.16 (17.34-35.01)$  %, correspondently. \*Significant difference ( $p \leq 0.05$ ) between outcome groups (PC vs NPC), Wilcoxon sum-rank test. †Significant difference ( $p \leq 0.05$ ) between time points, Friedman test followed the Bonferroni procedure. *ABT* = abnormal brain tissue; aSAH = aneurysmal subarachnoid hemorrhage; *ABTBBBD* = blood brain barrier damage measured in abnormal brain tissue volume; *NBTBBBD* = blood brain barrier damage measured in normal brain tissue volume; CI = confidence interval; *CSF* = cerebrospinal fluid; *LV* = lateral ventricles; *NBT* = normal brain tissue; *SAS* = subarachnoid space.

BBBD could be found in brain regions distant to the ABT, the highest probability of a BBB-disrupted voxel (comparably to non-BBB-disrupted) to turn into ABT was found at a distance of  $\leq 1$  cm from the ABT ( $p < 0.001$ , Kruskal-Wallis, Table 3). In contrast, the probability of a non-BBBD voxel to turn into ABT was significantly lower compared to a voxel with BBB and was not related to distance from ABT (Table 3).

### 3.4. Dynamics of intracranial measures reveals a progressive or non-progressive disease course

According to the dynamic changes found in tissue characteristics over time, patients were grouped into a “progressive” and “non-progressive” disease course (PC and NPC, respectively). PC was attributed to patients in whom the healthy brain tissue (NBT) volume decreased between the initial and last scan, while NPC was attributed to patients in whom the abnormal tissue volume decreased (Fig. 2b-c). In our cohort, 63% (78/124) of patients were classified as having a PC and 37% (46/124) displayed a NPC. No differences were found between the groups in distributions of gender, aneurysm location and type of intervention (Table 2). Importantly, the initial early scan ( $t1$ ) did not show differences between the groups in volume of ABT, LV or SAS.

Imaging-based categorization of disease course highly correlated with clinical outcome, as determined by eGOS, with a sensitivity of 98% and specificity of 97%: Forty-two (97.7%) patients with a non-progressive course had favorable eGOS, whereas 67 (97.1%) patients with a progressive course had poor eGOS. Thus, out of 112 patients, only three patients (2.68%) were misclassified: one patient with a gradual increase in the volume of apparently abnormal tissue showed a good outcome (eGOS = 6), and two patients with a decrease in measured abnormal tissue had a poor outcome (eGOS = 5). In contrast, disease course correlated poorly with clinical status on admission (sensitivity = 0.674, specificity = 0.654, appendix Table 3). The correspondence between aSAH course (PC/NPC groups) and WFNS categories was 64.5% (80/124 matched), and to RMS categories it was 70.2% (87/124 matched, sensitivity = 0.655, specificity = 0.716).

### 3.5. BBBD dynamics and clinical course

Interestingly, already at the very early scan ( $t1$ ) and in all investigation time points, brain volume with BBBD was significantly larger in the progressive course compared to the non-progressive disease course group ( $p = 0.001$ , Wilcoxon rank-sum test). When correlated with clinical status on admission (WFNS), we found that during all scanning time points, the extent of BBBD in abnormal brain tissue (ABT-BBBD) was associated with poor WFNS ( $p < 0.041$ , Wilcoxon rank-sum test). Notably, at all time points and in both NBT and ABT, BBBD was significantly larger in patients within the poor eGOS group ( $p < 0.001$ , Wilcoxon rank-sum test, Table 2).

### 3.6. Predictive value of clinical and imaging biomarkers with ROC analysis

We next used logistic regression models in search of clinical and imaging biomarkers that best predict aSAH outcome. Model fit and ROC analysis results for predicting long-term eGOS are shown in Table 4 and Fig. 3. When only clinical data were used, ROC analysis revealed a “fair” area under curve (AUC) for both models, consisting of either age and WFNS or RMS score only. Prediction was improved with addition of extent of BBBD in apparently normal brain tissue (BBBD-NBT) and volume of ABT.

## 4. Discussion

Cerebral ischemia after aSAH is a cause of substantial morbidity and mortality [28]. In the present study, we examined the potential of quantitative imaging, including imaging of BBBD, in predicting delayed tissue damage and clinical outcome. In this patient population with severe aSAH [29], we found that: (1) Disease progression occurred mostly during the first week, but the volume of abnormal tissue may continue to progress for months after the acute hemorrhagic insult; (2) Imaging-based measurements showing a progressive disease were associated with a worse clinical outcome at >6 months; (3) Significant BBB pathology can be detected as soon as 24–48 h after the acute bleeding, and was found within the apparently normal and abnormal brain tissue; (4) BBB pathology was widespread but most likely found in the apparently normal brain tissue surrounding the abnormal brain tissue; (5) BBB pathology may persist for months after the insult and was larger in patients with a progressive course; (6) Voxels with BBBD within the apparently

**Table 3**  
Investigation of a voxel fate:

Probability of turnover of a normal brain tissue voxel at $t1$ to turn into ABT at $t4$ :				
	ABT <sup>10</sup>	ABT <sup>20</sup>	ABT <sup>20</sup>	<i>n</i>
NBTBBBD <sub>1</sub>	0.284 <sup>*,***</sup> (0.122–0.594)	0.196 <sup>*</sup> (0.106–0.412)	0.212 <sup>*</sup> (0.099–0.464)	70
NBTBBBD <sub>1</sub>	0.089 (0.068–0.141)	0.063 (0.045–0.101)	0.069 (0.052–0.117)	70
Probability of persistence of an abnormal brain tissue voxel with BBBD to remain ABT at $t4$ :				
	Total			<i>n</i>
ABTBBBD <sub>1</sub>	0.697 (0.584–0.841)**			70
ABTBBBD <sub>2</sub>	0.721 (0.596–0.838)**			61
ABTBBBD <sub>3</sub>	0.740 (0.630–0.937)**			64
Probability of persistence of an abnormal brain tissue voxel without BBBD to remain ABT at $t4$ :				
	Total			<i>n</i>
ABTBBBD <sub>1</sub>	0.244 (0.102–0.348)			70
ABTBBBD <sub>2</sub>	0.252 (0.121–0.377)			61
ABTBBBD <sub>3</sub>	0.242 (0.114–0.353)			64

<sup>\*</sup>Significant difference between probabilities of a normal brain tissue (NBT) voxel with blood brain barrier damage (BBBD) (NBTBBBD<sub>1</sub>) and without BBBD (NBTBBBD<sub>1</sub>) to become an abnormal brain tissue (ABT<sub>4</sub>) voxel at  $t4$  ( $p < 0.05$ , Wilcoxon sum-rank test).

<sup>\*\*</sup>Significant difference between probabilities of ABT voxel with BBBD (ABTBBBD<sub>j</sub>) and without BBBD (ABTBBBD<sub>j</sub>) to remain an ABT<sub>4</sub> voxel at  $t4$  (where  $j = 1, \dots, 3$  denotes time interval  $t1-t3$ ) ( $p < 0.05$ , Wilcoxon sum-rank test).

<sup>\*\*\*</sup>Significant difference between different regions: ABT<sup>10</sup>, ABT<sup>20</sup> and ABT<sup>20</sup> ( $p < 0.05$ , Kruskal-Wallis test).

**Table 4**  
Models for long-term outcome prognoses:

Model	Coefficient	Coefficient Value (SE)	OR (95% CI)	p	n	AUC (SE)	
<b>A. Models for prediction course of aSAH<sup>a</sup></b>							
$\Psi_0^{WFNS}$	$\beta_1 * WFNS$	$\beta_1$	-0.445 (0.129)	0.64 (0.50-0.83)	0.001	124	0.673 (0.052)
$\Psi_0^{Age\&WFNS}$	$\beta_1 * Age + \beta_2 * WFNS$	$\beta_1$	-0.034 (0.018)	0.97 (0.93-1.00)	0.060	124	0.712 (0.049)
		$\beta_2$	-0.434 (0.130)	0.65 (0.50-0.84)	0.001		
$\Psi_0^{RMS}$	$\beta_1 * RMS$	$\beta_1$	-0.431 (0.113)	0.65 (0.52-0.81)	0.000	124	0.719 (0.048)
$\Psi_1$	$\beta_1 * NBTBBBD_1 + \beta_2 * RMS$	$\beta_1$	-0.035 (0.010)	0.97 (0.95-0.98)	0.000	93	0.829 (0.043)
		$\beta_2$	-0.348 (0.149)	0.71 (0.53-0.95)	0.020		
$\Psi_2$	$\beta_1 * NBTBBBD_2 + \beta_2 * WFNS$	$\beta_1$	-0.057 (0.018)	0.55 (0.33-0.94)	0.030	55	0.905 (0.042)
		$\beta_2$	-0.590 (0.272)	0.95 (0.91-0.98)	0.001		
$\Psi_3$	$\beta_1 * NBTBBBD_3$	$\beta_1$	-51.697 (13.931)	0.00 (0.00-0.00)	0.000	88	0.793 (0.049)
$\Psi_4$	$\beta_1 * ABT_4 + \beta_2 * NBTBBBD_4 + \beta_3 * ABTBBBD_4$	$\beta_1$	-0.138 (0.060)	0.87 (0.77-0.98)	0.022	46	0.979 (0.017)
		$\beta_2$	-0.059 (0.027)	0.94 (0.89-0.99)	0.027		
		$\beta_3$	0.298 (0.148)	1.35 (1.01-1.80)	0.044		
<b>B. Models for prediction of eGOS status of aSAH<sup>a</sup>:</b>							
$\Psi_0^{WFNS}$	$\beta_1 * WFNS$	$\beta_1$	-0.471 (0.138)	0.63 (0.48-0.82)	0.001	112	0.676 (0.055)
$\Psi_0^{Age\&WFNS}$	$\beta_1 * Age + \beta_2 * WFNS$	$\beta_1$	-0.062 (0.021)	0.94 (0.90-0.98)	0.003	112	0.750 (0.050)
		$\beta_2$	0.484 (-0.144)	0.62 (0.47-0.82)	0.001		
$\Psi_0^{RMS}$	$\beta_1 * RMS$	$\beta_1$	-0.564 (0.132)	0.57 (0.44-0.74)	0.000	112	0.757 (0.048)
$\Psi_1$	$\beta_1 * NBTBBBD_1 + \beta_2 * RMS$	$\beta_1$	-0.027 (0.009)	0.97 (0.96-0.99)	0.003	79	0.827 (0.051)
		$\beta_2$	-0.491 (0.168)	0.61 (0.44-0.85)	0.004		
$\Psi_2$	$\beta_1 * ABT_2 + \beta_2 * NBTBBBD_2$	$\beta_1$	-0.013 (0.007)	0.99 (0.97-1.00)	0.073	50	0.871 (0.052)
		$\beta_2$	-0.030 (0.012)	0.97 (0.95-0.99)	0.012		
$\Psi_3$	$\beta_1 * ABTBBBD_3 + \beta_2 * RMS$	$\beta_1$	-0.044 (0.014)	0.96 (0.93-0.98)	0.002	78	0.830 (0.048)
		$\beta_2$	-0.382 (0.169)	0.68 (0.49-0.95)	0.023		
$\Psi_4$	$\beta_1 * ABT_4 + \beta_2 * ABTBBBD_4$	$\beta_1$	-0.087 (0.030)	0.92 (0.86-0.97)	0.004	44	0.942 (0.035)
		$\beta_2$	0.156 (0.075)	1.17 (1.01-1.36)	0.037		

SE = standard error.

<sup>a</sup> Uncategorized WFNS and RMS grades were used in the logistic model. Since the neurological grades on admission RMS and WFNS are dependent [25] variables, only one of them can be included in the multivariate model at the time.

healthy brain, especially those located in close proximity to the ABT, were likely to become pathological; (7) Multi-linear regression model revealed a significant power for early detection of BBBB in predicting clinical outcome.

Demographic characteristics of the present aSAH cohort were consistent with previous studies. While females were twice more prone to aSAH, they were affected later in life compared to males [30–33]. MCA and anterior communicating artery (ACoA) were the most frequent aneurysm locations, with ACoA aneurysms more frequent in males and MCA aneurysms more frequent in females [31,34,35]. Although coiling has gained acceptance as an alternative to clipping for aSAH treatment, it remains elusive how the two procedures are compared in terms of outcomes [36]. In the present cohort, no differences were found between the interventions in imaging- or clinical-based

outcome. Investigation of clinical data revealed, that history of hypertension (~3.7 times is more likely), anemia (~4 times) and neurological scores WFNS (~4 times) and RMS (~9 times) at admission were detected as predictors for a poor clinical outcome.

We present here two novel, independent, semi-automatic and objective image analysis approaches for the identification of brain pathologies. The first was used for the detection and monitoring of brain lesions (ABT). Interpretation of abnormal brain tissue after aSAH is particularly challenging because of the multitude of pathological processes. For instance, cytotoxic edema after aSAH may result from the initial global ischemia, intracerebral hemorrhage, early or delayed focal cerebral ischemia, brain retraction or extra-ventricular drainage. In a similar fashion, findings of BBBB/vasogenic edema can be the radiological correlate of edema caused by the initial ischemia and reperfusion injury

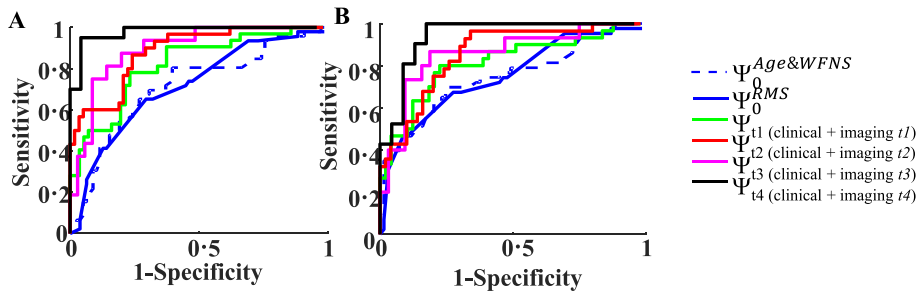


**Fig. 3.** Analysis of the predictive value of BBBB measurements in aSAH patients. Receiver operating characteristic (ROC) analysis showing specificity and sensitivity for prediction of aSAH course (a) and of long-term eGOS category (b). Whereas  $\Psi_0^{Age\&WFNS}$  (blue dashed line) and  $\Psi_0^{RMS}$  (blue solid line) models contain only clinical data, the remaining models combine clinical data with imaging results at the different time points ( $t1-t4$ ). When only clinical data was used, ROC analysis revealed a “fair” area under the curve (AUC) for the models consisting of either patient age and WFNS score ( $\Psi_0^{Age\&WFNS}$ : AUC = 0.712 for (a) and AUC = 0.750 for (b)), or of RMS score only ( $\Psi_0^{RMS}$ : AUC = 0.719 for (a) and AUC = 0.757 for (b)). Prediction was improved with addition of  $t1$  time-restricted imaging predictor, i.e. the extent of BBBB in apparently normal brain tissue ( $NBTBBBD_1$ ) and in volume of  $ABT_1$  ( $ABTBBBD_1$ ) ( $\Psi_{t1}$ : AUC = 0.829 for (a) and AUC = 0.827 for (b)). A better yet prediction was achieved with  $t2$  time-restricted models ( $\Psi_{t2}$ : correspondently: AUC = 0.905 and 0.871 for (a) and AUC = 0.855 and 0.887 for (b)). The best prediction was achieved with  $t4$  time-restricted model ( $\Psi_{t4}$ : AUC = 0.979 for (a) and AUC = 0.942 for (b)). While BBBB imaging alone revealed a “fair” prediction at  $t1$  (AUC = 0.724(0.059) for (a)AUC = 0.726(0.061) for (b)) and a “good” prediction at  $t2$  (AUC = 0.867(0.062) for (a)AUC = 0.816(0.073) for (b)). ABT = abnormal brain tissue; AUC = area under the curve; aSAH = aneurysmal subarachnoid hemorrhage;  $ABTBBBD$  = blood brain barrier damage measured in abnormal brain tissue volume;  $NBTBBBD$  = blood brain barrier damage measured in normal brain tissue volume.

leading to global cerebral edema, subarachnoid blood products, brain retraction during aneurysmal surgery, early or delayed focal cerebral ischemia, chronic white matter lesions or transependymal edema due to hydrocephalus. Therefore, based on multimodal signal intensities, anatomical location, and morphology, we used a general assessment of *ABT* to measure a sum of different pathogenic processes. We validated our approach by comparison to manual segmentation in a subset of aSAH patients (see appendix). Furthermore, the excellent correlation of disease progression with patients' clinical outcome confirms the validity of our analysis approach. It further suggests that, while most of the tissue damage occurs during the first week after bleeding, disease continues to progress for weeks and months.

Studies aimed at determining reliable biomarkers for the identification of patients at high risk for delayed complications following aSAH have been scarce. DeRoos and colleagues [37] developed a practical risk chart based solely on easily obtainable admission characteristics. Good clinical condition on admission (WFNS), small amount of extravasated blood and younger age were found to be associated with a low risk of delayed cerebral ischemia. However, the prediction model had poor specificity and sensitivity ( $AUC < 0.70$ ). Ayling and colleagues [28] found that presence of an early cerebral infarct, poor WFNS and greater subarachnoid clot were associated with poor outcome. However, the ability of early infarction to predict outcomes was also poor ( $AUC = 0.62$ ). In accordance with previous studies, we found that poor clinical condition on admission and advanced age are the earliest predictors of delayed increase in *ABT* [28,37–41]. In the present study, the predictive value of a model consisting of the significant predictor RMS was fair ( $AUC = 0.71$ ), greater than WFNS, and comparable to prognostic accuracy of a model combining WFNS with age. We show that MR-based quantitative analysis significantly improves the capacity to identify patients with disease progression (i.e. decline in *NBT*) and poor outcome. Importantly, we found that detection of *BBBD* as early as 24–48 h after the acute event improves model prediction. *BBBD* after aSAH has been described in human [42] and in a number of animal studies [43–45]. Based on animal experiments, *BBBD* has been suggested to play a key role in neuro-inflammation, astroglial activation and network modification, epileptogenesis and neurodegeneration [12,46,47]. These data suggest a direct link between *BBBD* and long-term outcome.

This is the first clinical study testing the potential of quantitative *BBBD* imaging in identifying patients at-risk for disease progression. We report that *BBBD* is common in aSAH patients and is found in both the apparently healthy and abnormal brain tissue. Our findings are in agreement with pre-clinical experiments showing that disease progression overlaps spatially and follows temporally *BBB* pathology [48]. A substantial part of lesions observed after aSAH involves the cerebral cortex [49], and lesions typically develop adjacent to subarachnoid blood clots in both animals and humans [50,51]. Therefore, it has been suggested that subarachnoid blood products are an important pathophysiological elements, likely through constrictive effects on small cortical arteries, depolarizing effects on cortical neurons and astrocytes and disturbed functional coupling between the different cellular elements within the neurovascular unit [52]. An additional effect of blood might be *BBB* opening through factors such as potassium and/or hemoglobin released from erythrocytes [53]. Thus, as supported by the present study, *BBBD* may serve as an indicator for tissue at risk to develop ischemia in response to subarachnoid blood clots.

We thus suggest *BBBD* imaging as a potential novel diagnostic and predictive biomarker for tissue at risk to develop ischemia in response to subarachnoid hemorrhage for the following reasons: (1) *BBB* permeability increase can be detected as early as 24 h after the acute insult; (2) Brain volume with *BBBD* is found in patients with a progressive disease, and was the only differentiating factor between the groups at the early time point ( $t_1$ ); (3) Apparently normal brain tissue with *BBBD* is likely to become abnormal with time; and (4) Inclusion of early *BBBD* within the normal brain tissue in a regression model improves prediction of outcome. With the accumulation of data on vascular protecting

therapy, it is not unlikely that microvascular pathology will become a target for early preventive treatment of patients after brain injury, further stressing the importance of quantitative diagnosis of vascular integrity.

This study had several limitations. First, *ABT*, detected by our algorithm, represents a mixture of different pathophysiological processes, including edema, hemorrhage and scar tissue. Future developments and identification of specific pathologies is expected to increase imaging sensitivity in predicting outcome, shed light on pathophysiological mechanisms in individual patients and offer specific treatment targets. Second, the study design posed difficulties such as unavailability of imaging data for all of the patients at all time points. Third, eGOS data were missing for ~10% of the patients. Only differences in frequencies of about 26% or more could be detected with sufficient power in this study. Nevertheless, despite of small sample size ( $n = 124$ ) this is the first large-scale study within the research field on *BBB* spatiotemporal course and lesion progression in patients with brain injury, offering new quantitative neuroimaging analysis methods that are informative for patient monitoring and outcome prediction. To conclude, we highlighted micro-vascular pathology and specifically a leaky *BBB* as a potential mechanism underlying disease progression as well as a diagnostic and predictive biomarker. Future prospective studies are awaited to test and validate our approach following traumatic and ischemic brain injuries before contrast-enhanced MRI should be recommended as routine test in patients after brain injuries.

#### Declaration of interests

All authors declare no competing interests.

#### Role of the funding source

The funders of the study had no role in study design, data collection, data analysis, data interpretation, or writing of the report. All authors had full access to all the data in the study and corresponding author had final responsibility for the decision to submit for publication.

#### Contributors

All authors contributed to the idea for design of the study and data acquisition, reviewed and approved the final manuscript. SL had responsibility for data analysis and writing of the first draft of the manuscript. SL and PM performed statistical analysis of the data. AF and JPD came up with the concept and design for the study, and were responsible for study supervision and funding.

#### Acknowledgments

The study was designed and performed as a sub-study within the Cooperative Study of Brain Injury Depolarizations (COSBID) study group. JPD was supported by grants from the Deutsche Forschungsgemeinschaft (DFG) (DFG DR 323/5-1), the Bundesministerium für Bildung und Forschung (BMBF) Center for Stroke Research Berlin 01 EO 0801 and FP7 no 602150 CENTER-TBI. AF was supported by grants from the DFG (DFG DR 323/5-1), Israel Science Foundation, Canada Institute for Health Research (CIHR) and the European Union's Seventh Framework Program (FP7/2007–2013; grant #602102). JW was supported by grants from the DFG DR 323/5-1 and DFG WO 1704/1-1.

#### Appendix A. Supplementary data

Supplementary data to this article can be found online at <https://doi.org/10.1016/j.ebiom.2019.04.054>.

## References

- [1] van Gijn J, Kerr RS, Rinkel GJ. Subarachnoid haemorrhage. *Lancet* Jan 27, 2007;369(9558):306–18 Internet. cited 2017 Jul 9. Available from <http://www.ncbi.nlm.nih.gov/pubmed/17258671>.
- [2] Feigin VL, Rinkel GJE, Lawes CMM, Algra A, Bennett DA, van Gijn J, et al. Risk factors for subarachnoid hemorrhage. *Stroke* 2005;36(12) Internet. cited 2017 Jul 9. Available from <http://stroke.ahajournals.org/content/36/12/2773.full>.
- [3] Hong CM, Tosun C, Kurland DB, Gerzanich V, Schreiberman D, Simard JM. Biomarkers as outcome predictors in subarachnoid hemorrhage—a systematic review. *Biomarkers Mar*, 2014;19(2):95–108 [Internet]. NIH Public Access. cited 2017 Jul 9. Available from <http://www.ncbi.nlm.nih.gov/pubmed/24499240>.
- [4] Dreier JP, Fabricius M, Ayata C, Sakowitz OW, William Shuttleworth C, Dohmen C, et al. Recording, analysis, and interpretation of spreading depolarizations in neurointensive care: review and recommendations of the COSBID research group. *J Cereb Blood Flow Metab* 2017;37(5).
- [5] Dreier JP, Lemale CL, Kola V, Friedman A, Schoknecht K. Spreading depolarization is not an epiphenomenon but the principal mechanism of the cytotoxic edema in various gray matter structures of the brain during stroke. *Neuropharmacology* May 15, 2018;134(Pt B):189–207 Internet. cited 2018 Jun 2. Available from: <http://www.ncbi.nlm.nih.gov/pubmed/28941738>.
- [6] Claassen J, Carhuapoma JR, Kreiter KT, Du EY, Connolly ES, Mayer SA. Global cerebral edema after subarachnoid hemorrhage. *Stroke* 2002;33(5) Internet. cited 2017 Jul 9. Available from <http://stroke.ahajournals.org/content/33/5/1225.long>.
- [7] Ostrowski RP, Colohan AR, Zhang JH. Molecular mechanisms of early brain injury after subarachnoid hemorrhage. *Neurol Res* Jun 19, 2006;28(4):399–414 [Internet]. Taylor & Francis. cited 2017 Jul 9. Available from: <http://www.tandfonline.com/doi/full/10.1179/016164106X115008>.
- [8] Song J-N, Chen H, Zhang M, Zhao Y-L, Ma X-D. Dynamic change in cerebral microcirculation and focal cerebral metabolism in experimental subarachnoid hemorrhage in rabbits. *Metab Brain Dis* Mar 12, 2013;28(1):33–43 [Internet]. Springer US. cited 2017 Jul 9. Available from: <http://link.springer.com/10.1007/s11011-012-9369-8>.
- [9] Gu H, Fei Z-H, Wang Y-Q, Yang J-G, Zhao C-H, Cai Y, et al. Angiopietin-1 and angiopietin-2 expression imbalance influence in early period after subarachnoid hemorrhage. *Int Neurourol J* Dec, 2016;20(4):288–95 [Internet]. Korean Continence Society. cited 2017 Jul 9. Available from: <http://www.ncbi.nlm.nih.gov/pubmed/28043115>.
- [10] Ivanidze J, Ferraro RA, Giambrone AE, Segal AZ, Gupta A, Sanelli PC. Blood-brain barrier permeability in aneurysmal subarachnoid hemorrhage: correlation with clinical outcomes. *Am J Roentgenol* Oct 7, 2018;211(4):891–5 [Internet]. American Roentgen Ray Society. cited 2018 Oct 20. Available from: <https://www.ajronline.org/doi/10.2214/AJR.17.18237>.
- [11] Russin JJ, Montagne A, D'Amore F, He S, Shiroishi MS, Rennett RC, et al. Permeability imaging as a predictor of delayed cerebral ischemia after aneurysmal subarachnoid hemorrhage. *J Cereb Blood Flow Metab* Jun 3, 2018;38(6):973–9 Internet. cited 2018 Jul 9. Available from: <http://www.ncbi.nlm.nih.gov/pubmed/29611451>.
- [12] Friedman A, Kaufner D, Heinemann U. Blood-brain barrier breakdown-inducing astrocytic transformation: novel targets for the prevention of epilepsy. *Epilepsy Res* Aug, 2009;85(2–3):142–9 Internet. cited 2015 Apr 7. Available from: <http://www.pubmedcentral.nih.gov/articlerender.fcgi?artid=3615244&tool=pmcentrez&rendertype=abstract>.
- [13] Bar-Klein G, Lublinsky S, Kaminsky L, Noyman I, Veksler R, Dalipaj H, et al. Imaging blood-brain barrier dysfunction as a biomarker for epileptogenesis. *Brain* Jun 1, 2017;140(6):1692–705 Internet. cited 2017 Jul 10. Available from: <http://www.ncbi.nlm.nih.gov/pubmed/28444141>.
- [14] Shlosberg D, Benifla M, Kaufner D, Friedman A. Blood-brain barrier breakdown as a therapeutic target in traumatic brain injury. *Nat Rev Neurol* Jul 15, 2010;6(7):393–403 Internet. cited 2017 Aug 7. Available from <http://www.nature.com/doi/10.1038/nrneuro.2010.74>.
- [15] Tomkins O, Friedman O, Ivens S, Reiffurth C, Major S, Dreier JP, et al. Blood-brain barrier disruption results in delayed functional and structural alterations in the rat neocortex. *Neurobiol Dis* Feb, 2007;25(2):367–77 Internet. cited 2017 Aug 7. Available from <http://www.ncbi.nlm.nih.gov/pubmed/17188501>.
- [16] Tomkins O, Feintuch A, Benifla M, Cohen A, Friedman A, Shelef I. Blood-brain barrier breakdown following traumatic brain injury: a possible role in posttraumatic epilepsy. *Cardiovasc Psychiatry Neurol* Jan, 2011;2011:765923 Internet. cited 2015 Feb 18. Available from: <http://www.pubmedcentral.nih.gov/articlerender.fcgi?artid=3056210&tool=pmcentrez&rendertype=abstract>.
- [17] Chassidim Y, Vazana U, Prager O, Veksler R, Bar-Klein G, Schoknecht K, et al. Analyzing the blood-brain barrier: the benefits of medical imaging in research and clinical practice. *Semin Cell Dev Biol* Nov 29, 2014 Internet. [cited 2015 Feb 18]; Available from: <http://www.ncbi.nlm.nih.gov/pubmed/25455024>.
- [18] Tofts PS. Modeling tracer kinetics in dynamic Gd-DTPA MR imaging. *J Magn Reson Imaging* Jan, 1997;7(1):91–101 Internet. cited 2015 Apr 5. Available from: <http://www.ncbi.nlm.nih.gov/pubmed/9039598>.
- [19] Tofts PS, Kermode AG. Measurement of the blood-brain barrier permeability and leakage space using dynamic MR imaging. 1. Fundamental concepts. *Magn Reson Med* Feb, 1991;17(2):357–67 Internet. cited 2017 Aug 7. Available from: <http://www.ncbi.nlm.nih.gov/pubmed/2062210>.
- [20] Chassidim Y, Veksler R, Lublinsky S, Pell GS, Friedman A, Shelef I. Quantitative imaging assessment of blood-brain barrier permeability in humans. *Fluids Barriers CNS* Jan, 2013;10(1):9 Internet. cited 2015 Jan 23. Available from: <http://www.pubmedcentral.nih.gov/articlerender.fcgi?artid=3570379&tool=pmcentrez&rendertype=abstract>.
- [21] Weissberg I, Reichert A, Heinemann U, Friedman A. Blood-brain barrier dysfunction in epileptogenesis of the temporal lobe. *Epilepsy Res Treat* 2011;2011:1–10.
- [22] Winkler MK, Dengler N, Hecht N, Hartings JA, Kang EJ, Major S, et al. Oxygen availability and spreading depolarizations provide complementary prognostic information in neuromonitoring of aneurysmal subarachnoid hemorrhage patients. *J Cereb Blood Flow Metab* May 20, 2017;37(5):1841–56 Internet. cited 2018 Jun 2. Available from <http://www.ncbi.nlm.nih.gov/pubmed/27025768>.
- [23] Dreier JP, Major S, Manning A, Woitzik J, Drenckhahn C, Steinbrink J, et al. Cortical spreading ischaemia is a novel process involved in ischaemic damage in patients with aneurysmal subarachnoid haemorrhage. *Brain* Jul 1, 2009;132(7):1866–81 Internet. cited 2018 Dec 16. Available from <http://www.ncbi.nlm.nih.gov/pubmed/19420089>.
- [24] Drake CG. Report of World Federation of Neurological Surgeons Committee on a universal subarachnoid hemorrhage grading scale. *J Neurosurg* Jun, 1988;68(6):985–6 Internet. cited 2017 Aug 7. Available from <http://www.ncbi.nlm.nih.gov/pubmed/3131498>.
- [25] Rosen DS, Macdonald RL. Grading of subarachnoid hemorrhage: modification of the world World Federation of Neurological Societies scale on the basis of data for a large series of patients. *Neurosurgery* Mar, 2004;54(3):566–75 Internet. cited 2018 Feb 7. discussion 575–6. Available from: <http://www.ncbi.nlm.nih.gov/pubmed/15028129>.
- [26] Vora YY, Suarez-Almazor M, Steinke DE, Martin ML, Findlay JM. Role of transcranial Doppler monitoring in the diagnosis of cerebral vasospasm after subarachnoid hemorrhage. *Neurosurgery* Jun, 1999;44(6):1237–47 Internet. cited 2018 Jan 24. discussion 1247–8. Available from: <http://www.ncbi.nlm.nih.gov/pubmed/10371622>.
- [27] Safari S, Baratloo A, Elfil M, Negida A. Evidence based emergency medicine; part 5 receiver operating curve and area under the curve. *Emerg (Tehran, Iran)* 2016;4(2):111–3 [Internet]. Shahid Beheshti University of Medical Sciences; [cited 2018 Dec 27]. Available from: <http://www.ncbi.nlm.nih.gov/pubmed/27274525>.
- [28] Ayling OGS, Ibrahim GM, Alotaibi NM, Gooderham PA, Macdonald RL. Dissociation of early and delayed cerebral infarction after subarachnoid hemorrhage. *Stroke* Dec, 2016;47(12):2945–51 Internet. cited 2017 Sep 16. Available from <http://www.ncbi.nlm.nih.gov/pubmed/27827324>.
- [29] Dreier JP, Woitzik J, Fabricius M, Bhatia R, Major S, Drenckhahn C, et al. Delayed ischaemic neurological deficits after subarachnoid haemorrhage are associated with clusters of spreading depolarizations. *Brain* Jun 9, 2006;129(12):3224–37 Internet. cited 2018 Jun 2. Available from <http://www.ncbi.nlm.nih.gov/pubmed/17067993>.
- [30] Park SK, Kim JM, Kim JH, Cheong JH, Bak KH, Kim CH. Aneurysmal subarachnoid hemorrhage in young adults: a gender comparison study. *J Clin Neurosci* Apr, 2008;15(4):389–92 Internet. cited 2017 Aug 24. Available from <http://www.ncbi.nlm.nih.gov/pubmed/18242092>.
- [31] Ghods AJ, Lopes D, Chen M. Gender differences in cerebral aneurysm location. *Front Neurol* 2012;3(78) [Internet]. Frontiers Media SA. cited 2017 Aug 24. Available from: <http://www.ncbi.nlm.nih.gov/pubmed/22661965>.
- [32] Eden SV, Meurer WJ, Sánchez BN, Lisabeth LD, Smith MA, Brown DL, et al. Gender and ethnic differences in subarachnoid hemorrhage. *Neurology* Sep 2, 2008;71(10):731–5 [Internet]. American Academy of Neurology. cited 2017 Aug 24. Available from: <http://www.ncbi.nlm.nih.gov/pubmed/18550859>.
- [33] Horiuchi T, Tanaka Y, Hongo K. Sex-related differences in patients treated surgically for aneurysmal subarachnoid hemorrhage. *Neurol Med Chir (Tokyo)* Jul, 2006;46(7):328–32 Internet. cited 2017 Aug 24. discussion 332. Available from: <http://www.ncbi.nlm.nih.gov/pubmed/16861825>.
- [34] Lindner SH, Bor ASE, Rinkel GJE. Differences in risk factors according to the site of intracranial aneurysms. *J Neurol Neurosurg Psychiatry* Jan 1, 2010;81(1):116–8 Internet. cited 2017 Sep 16. Available from <http://www.ncbi.nlm.nih.gov/pubmed/20019231>.
- [35] Wermer MJH, van der Schaaf IC, Algra A, Rinkel GJE. Risk of rupture of unruptured intracranial aneurysms in relation to patient and aneurysm characteristics. *Stroke* 2007;38(4) Internet. cited 2017 Sep 16. Available from <http://stroke.ahajournals.org/content/38/4/1404>.
- [36] Yoon W. Current update on the randomized controlled trials of intracranial aneurysms. *Neurointervention* Feb 1, 2011;6(1):1 Internet. cited 2017 Sep 24. Available from: <https://synapse.koreamed.org/DOLx.php?id=10.5469/neuroint.2011.6.1.1>.
- [37] de Rooij NK, Greving JP, Rinkel GJE, Frijns CJM. Early prediction of delayed cerebral ischemia after subarachnoid hemorrhage: development and validation of a practical risk chart. *Stroke* May 1, 2013;44(5):1288–94 Internet. cited 2017 Sep 2. Available from <http://www.ncbi.nlm.nih.gov/pubmed/23512975>.
- [38] Adams HP, Kassell NF, Torner JC, Haley EC. Predicting cerebral ischemia after aneurysmal subarachnoid hemorrhage: influences of clinical condition, CT results, and antifibrinolytic therapy. A report of the cooperative aneurysm study. *Neurology* Oct, 1987;37(10):1586–91 Internet. cited 2017 Sep 2. Available from <http://www.ncbi.nlm.nih.gov/pubmed/3658161>.
- [39] Fisher CM, Kistler JP, Davis JM. Relation of cerebral vasospasm to subarachnoid hemorrhage visualized by computerized tomographic scanning. *Neurosurgery* Jan, 1980;6(1):1–9 Internet. cited 2017 Sep 2. Available from <http://www.ncbi.nlm.nih.gov/pubmed/7354892>.
- [40] Lanzino G, Kassell NF, Germanson TP, Kongable GL, Truskowski LL, Torner JC, et al. Age and outcome after aneurysmal subarachnoid hemorrhage: why do older patients fare worse? *J Neurosurg* Sep, 1996;85(3):410–8 Internet. cited 2017 Sep 24. Available from <http://www.ncbi.nlm.nih.gov/pubmed/8751625>.
- [41] Degos V, Gourraud P-A, Tursis VT, Whelan R, Colonne C, Korinek AM, et al. Elderly age as a prognostic marker of 1-year poor outcome for subarachnoid Hemorrhage patients through its interaction with admission hydrocephalus. *Anesthesiology* Dec, 2012;117(6):1289–99 Internet. cited 2017 Sep 24. Available from <http://www.ncbi.nlm.nih.gov/pubmed/22854979>.

- [42] Dóczi T. The pathogenetic and prognostic significance of blood-brain barrier damage at the acute stage of aneurysmal subarachnoid haemorrhage. Clinical and experimental studies. *Acta Neurochir* 1985;77(3–4):110–32 Internet. cited 2017 Sep 24. Available from: <http://www.ncbi.nlm.nih.gov/pubmed/4072781>.
- [43] Trojanowski T. Blood-brain barrier changes after experimental subarachnoid haemorrhage. *Acta Neurochir Mar*, 1982;60(1–2):45–54 [Internet]. Springer-Verlag. cited 2017 Sep 24. Available from: <http://link.springer.com/10.1007/BF01401749>.
- [44] Germanò A, d'Avella D, Imperatore C, Caruso G, Tomasello F. Time-course of blood-brain barrier permeability changes after experimental subarachnoid haemorrhage. *Acta Neurochir* 2000;142(5):575–80 Internet. cited 2017 Sep 24. discussion 580–1. Available from <http://www.ncbi.nlm.nih.gov/pubmed/10898366>.
- [45] Schöller K, Trinkl A, Klopotoski M, Thal SC, Plesnila N, Trabold R, et al. Characterization of microvascular basal lamina damage and blood-brain barrier dysfunction following subarachnoid hemorrhage in rats. *Brain Res Apr* 20, 2007;1142:237–46 Internet. cited 2017 Sep 24. Available from <http://www.ncbi.nlm.nih.gov/pubmed/17303089>.
- [46] Friedman A, Kaufer D. Blood-brain barrier in health and disease. *Semin Cell Dev Biol Feb*, 2015;38(1) Internet. cited 2017 Jul 10. Available from <http://linkinghub.elsevier.com/retrieve/pii/S108495211500049X>.
- [47] Lippmann K, Kamintsky L, Kim SY, Lublinsky S, Prager O, Nichtweiss JF, et al. Epileptiform activity and spreading depolarization in the blood-brain barrier-disrupted peri-infarct hippocampus are associated with impaired GABAergic inhibition and synaptic plasticity. *J Cereb Blood Flow Metab May* 1, 2017;37(5):1803–19 [Internet]. SAGE Publications Sage UK: London, England. cited 2017 Jul 10. Available from: <http://journals.sagepub.com/doi/10.1177/0271678X16652631>.
- [48] Schoknecht K, Prager O, Vazana U, Kamintsky L, Harhausen D, Zille M, et al. Monitoring stroke progression: in vivo imaging of cortical perfusion, blood-brain barrier permeability and cellular damage in the rat photothrombosis model. *J Cereb Blood Flow Metab* 2014;34:1791–801.
- [49] Neil-Dwyer G, Lang DA, Doshi B, Gerber CJ, Smith PW. Delayed cerebral ischaemia: the pathological substrate. *Acta Neurochir* 1994;131(1–2):137–45 Internet. cited 2018 Jun 2. Available from: <http://www.ncbi.nlm.nih.gov/pubmed/7709776>.
- [50] Hartings JA, York J, Carroll CP, Hinzman JM, Mahoney E, Krueger B, et al. Subarachnoid blood acutely induces spreading depolarizations and early cortical infarction. *Brain Oct* 1, 2017;140(10):2673–90 Internet. cited 2018 Jun 2. Available from <https://academic.oup.com/brain/article/140/10/2673/4102114>.
- [51] Stoltenberg-Didinger G, Schwarz K. Brain lesions secondary to subarachnoid hemorrhage due to ruptured aneurysms. In: Cervos-Navarro J, Ferszt R, editors. *Stroke and microcirculation*. New York: Raven Press; 1987. p. 471–80.
- [52] Dreier JP. The role of spreading depression, spreading depolarization and spreading ischemia in neurological disease. *Nat Med Apr* 7, 2011;17(4):439–47 Internet. cited 2018 Jun 2. Available from <http://www.ncbi.nlm.nih.gov/pubmed/21475241>.
- [53] Ohta O, Osaka K, Siguma M, Yamamoto M, Shimizu K, Toda N. Cerebral vasospasm following ruptured intracranial aneurysms, especially some contributions of potassium ion released from subarachnoid hematoma to delayed cerebral vasospasm. In: Bevan SA, editor. *Vascular neuroeffector mechanisms*. New York: Raven Press; 1983 p. 535–358.